RESEARCH ARTICLE SUMMARY

STRUCTURAL BIOLOGY

Evolutionary shift toward protein-based architecture in trypanosomal mitochondrial ribosomes

David J. F. Ramrath*, Moritz Niemann*, Marc Leibundgut, Philipp Bieri, Céline Prange, Elke K. Horn, Alexander Leitner, Daniel Boehringer, André Schneider, Nenad Ban†

INTRODUCTION: Ribosomes are universally conserved assemblies composed of ribosomal RNA (rRNA) and proteins, where rRNA plays key structural and functional roles. Despite their high degree of conservation, considerable variability is observed in mitochondrial ribosomes (mitoribosomes), with an extreme example found in *Trypanosoma brucei*, the parasite that causes sleeping sickness. In these mitoribosomes featuring the smallest known rRNAs, the severe rRNA reduction is accompanied by the recruitment of many additional proteins.

RATIONALE: The extreme differences in rRNA size and the substitution of many proteins present in all other ribosomes render trypanosomal mitoribosomes an excellent system to reveal the minimal set of rRNA and protein elements essential for ribosomal function and to investigate how ribosomal proteins compensated for the missing rRNA. To address these questions, we determined the atomic structure of the mitoribosome from *T. brucei* using cryo–electron microscopy.

RESULTS: The trypanosomal mitoribosome, composed of 127 ribosomal proteins and two rRNAs, is larger and architecturally more complex than any other ribosome described so far with a molecular weight of 4.5 MDa and a RNA/protein ratio of 1:6. The structural changes are most prominent in the small subunit that exceeds the size of the "large" subunit. Notably, the reduced rRNA is found at the core of the assembly and is encased in a large shell of mitoribosomal proteins. The universally conserved regions are reduced to a minimum and include only a few rRNA and protein elements in the vicinity of key functional regions of the ribosome, namely, the decoding center, the active site, and the binding region for translation factors.

ON OUR WEBSITE

Read the full article at http://dx.doi.org/10.1126/science.aau7735

In contrast to other ribosomes, where the rRNA fold is dominated by a base-paired structure, the proteins take over the architectural role by providing a scaffold for binding of predominantly single-stranded rRNA. The switch to the protein-based architecture is accompanied by a marked increase in the size of conserved ribosomal proteins and the recruitment of novel proteins, including proteins with multiple domains or proteins with homology to various enzymes. Because many proteins contain helical repeat motifs, the assembly contains a disproportionately large fraction of α-helical elements that structurally substitute the reduced rRNA.

Our results show that, because of the extensive remodeling, the trypanosomal translational machinery adopted unusual solutions to accomplish some basic protein synthesis mechanisms. Their nascent polypeptide exit tunnel branches into two exits providing for an interesting possibility that nascent proteins with different characteristics may take different paths. Furthermore, in a subpopulation of isolated small-subunit particles, we observed mitochondrial initiation factor 3 interacting with the decoding center via its unique C-terminal extension, which might compensate for the essential function of initiation factor 1 that is absent in all mitochondria.

CONCLUSION: The unusual architecture and composition of the trypanosomal mitoribosome that we have revealed shows how proteins have taken over a key architectural role from rRNA by forming an autonomous outer shell that serves as a mold for binding flexible single-stranded rRNAs. Moreover, our results show the universally conserved features of ribosomes that are responsible for the most basic functions. Last, structural information on these ribosomes may be helpful for developing new drugs to treat sleeping sickness and other diseases caused by trypanosomes and its relatives. ■

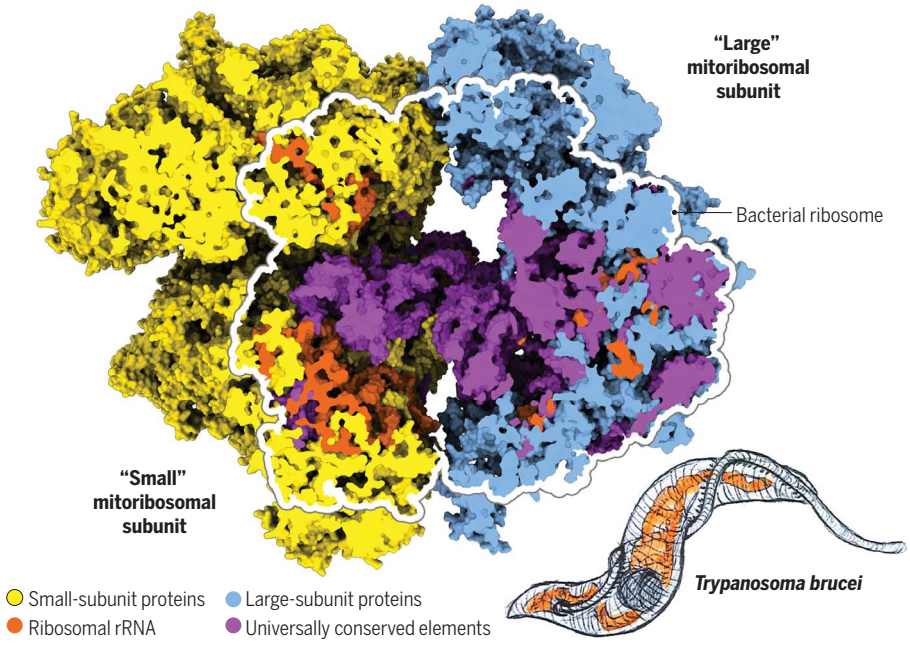

The universally conserved core of the ribosome. In the highly remodeled trypanosomal mitoribosome, where the "small" subunit is larger than the large subunit, proteins took over the key architectural role from the rRNA. The massive protein shell interacts with the extremely reduced rRNA to position functionally critical rRNA elements. The structure helps us define the "minimal" set of conserved rRNA regions and protein components shared by all ribosomes.

The list of author affiliations is available in the full article online.
*These authors contributed equally to this work.
†Corresponding author. Email: ban@mol.biol.ethz.ch
Cite this article as D. J. F. Ramrath *et al.*, *Science* **362**, eaau7735 (2018). DOI: 10.1126/science.aau7735

RESEARCH ARTICLE

STRUCTURAL BIOLOGY

Evolutionary shift toward protein-based architecture in trypanosomal mitochondrial ribosomes

David J. F. Ramrath[1]*, Moritz Niemann[2]*, Marc Leibundgut[1], Philipp Bieri[1], Céline Prange[1], Elke K. Horn[2], Alexander Leitner[3], Daniel Boehringer[1], André Schneider[2], Nenad Ban[1]†

Ribosomal RNA (rRNA) plays key functional and architectural roles in ribosomes. Using electron microscopy, we determined the atomic structure of a highly divergent ribosome found in mitochondria of *Trypanosoma brucei*, a unicellular parasite that causes sleeping sickness in humans. The trypanosomal mitoribosome features the smallest rRNAs and contains more proteins than all known ribosomes. The structure shows how the proteins have taken over the role of architectural scaffold from the rRNA: They form an autonomous outer shell that surrounds the entire particle and stabilizes and positions the functionally important regions of the rRNA. Our results also reveal the "minimal" set of conserved rRNA and protein components shared by all ribosomes that help us define the most essential functional elements.

Ribosomal RNA (rRNA) plays key functional and architectural roles in ribosomes. Using electron microscopy, we determined the atomic structure of a highly divergent ribosome found in mitochondria of *Trypanosoma brucei*, a unicellular parasite that causes sleeping sickness in humans. The trypanosomal mitoribosome features the smallest rRNAs and contains more proteins than all known ribosomes. The structure shows how the proteins have taken over the role of architectural scaffold from the rRNA: They form an autonomous outer shell that surrounds the entire particle and stabilizes and positions the functionally important regions of the rRNA. Our results also reveal the "minimal" set of conserved rRNA and protein components shared by all ribosomes that help us define the most essential functional elements.

Ribosomes are two-subunit ribonucleoprotein assemblies responsible for protein synthesis in all organisms and are considered among the most conserved cellular complexes (*1*). Consequently, the sequence of the bacterial small-subunit 16*S* rRNA has traditionally been used to establish evolutionary relationships between organisms (*2*, *3*). Structural information on ribosomes from different kingdoms of life revealed a conserved ribosomal core where the peptidyl transferase center (PTC) and the decoding center are formed by rRNA, whereas surface features vary in terms of protein composition and lengths of rRNA expansion segments to account for different regulatory mechanisms that control translation in different organisms (*4*). So far, the most pronounced structural deviation from bacteria is found in mammalian mitochondria. These mitoribosomes are specialized for the synthesis of membrane proteins and feature a reduced rRNA and increased protein content (*5*, *6*). Notably, an even more extreme rRNA reduction is found in mitochondria of kinetoplastids such as *T. brucei*, *Trypanosoma cruzi*, and *Leishmania* sp., the parasites that, in humans, cause sleeping sickness, Chagas disease, and Leishmaniasis. Their mitoribosomal small-subunit 9*S* and large-subunit 12*S* rRNA (comprising 620 and 1176 nucleotides, respectively, in *T. brucei*) are the smallest known rRNA homologs, reduced to ~40% of the length of canonical eubacterial rRNA (*7*–*9*). The trypanosomal mitochondrial rRNA sequences have an ~80% adenine and uracil content, which hampers the prediction of secondary structure elements that are otherwise present in all rRNAs (*9*). Proteomic studies of affinity-purified trypanosomal mitoribosomes indicate that the rRNA reduction was accompanied by the recruitment of many additional mitoribosomal proteins; however, it was not possible to obtain clear information regarding their size or regarding the number of ribosomal proteins that compose their subunits (*10*–*12*). Nevertheless, these results indicated that trypanosomal mitoribosomes have a unique composition and architecture distinct from any other cytoplasmic and mitochondrial ribosomes (*5*, *6*, *13*, *14*).

The extent of anticipated architectural differences in trypanosomal mitoribosomes render it an excellent system to establish the most conserved set of rRNA and protein elements essential for ribosomal function and to reveal possible changes in the rRNA, which dominates the architecture of all currently investigated ribosomes. Here, we present the cryo–electron microscopy (cryo-EM) structures of both mitoribosomal subunits of the parasitic protozoan *T. brucei* at 3.1- to 3.4-Å resolution in the context of the entire trypanosomal mitoribosome resolved at 7.8 Å. Our reconstructions reveal the unique composition and the unusual protein-based architecture of trypanosomal mitoribosomes.

Results

Sample preparation, structure determination, and model building

Because of the low abundance of kinetoplastid mitoribosomes and their unusual heterogeneity (*10*), they were purified using genetically engineered PTP affinity tags (*15*). However, without knowing the exact composition and architecture of these mitoribosomes, we had to iteratively improve the placement of the tags based on preliminary structural information. From purified mitoribosomes that carried either a large- or small-subunit tag exposed on the solvent accessible side of the particle (fig. S1), we acquired two cryo-EM datasets, which were subsequently processed by several rounds of two-dimensional (2D) and 3D classification steps (fig. S2).

This approach yielded maps of the entire *T. brucei* mitoribosome, its small (Tb-mt-SSU) and large (Tb-mt-LSU) subunits and a distinct class of small subunits in complex with the C-terminal domain (CTD) of initiation factor IF-3 (Tb-mt-SSU•IF-3). For the final high-resolution refinements, individual masks for the Tb-mt-LSU and the Tb-mt-SSU head and body further improved the map quality, resulting in cryo-EM maps at overall resolutions of 3.1 Å for the Tb-mt-SSU head, 3.3 Å for Tb-mt-SSU•IF-3 body, and 3.4 Å for the Tb-mt-LSU (Fig. 1A, figs. S2 and S3, and table S1). Most novel proteins were identified by predicting their sequence based on the side-chain features in EM maps, followed by sequence homology search, 3D modeling, and manual rebuilding. The resulting hits were further corroborated by comparison with the mass spectrometry data that we have collected (data S1). Most of the rRNA segments were readily visible; however, some regions of the 9*S* and 12*S* rRNA at the subunit interface were flexibly disposed, which precluded a molecular interpretation. In the case of the small ribosomal subunit, the complete 9*S* rRNA structure could be determined using the Tb-mt-SSU•IF-3 map, where these areas were well ordered. The missing regions of the large-subunit 12*S* rRNA were modeled for display purposes using the structure of the mammalian mitoribosomal 16*S* rRNA as a guide based on sequence and secondary structure homology (Fig. 1B) (*5*, *6*). On the surface of the mitoribosomal subunits, and at

[1]Department of Biology, Institute of Molecular Biology and Biophysics, Otto-Stern-Weg 5, ETH Zurich, CH-8093 Zurich, Switzerland. [2]Department of Chemistry and Biochemistry, University of Bern, CH-3012 Bern, Switzerland. [3]Department of Biology, Institute of Molecular Systems Biology, Auguste-Piccard-Hof 1, ETH Zurich, CH-8093 Zurich, Switzerland.
*These authors contributed equally to this work.
†Corresponding author. Email: ban@mol.biol.ethz.ch

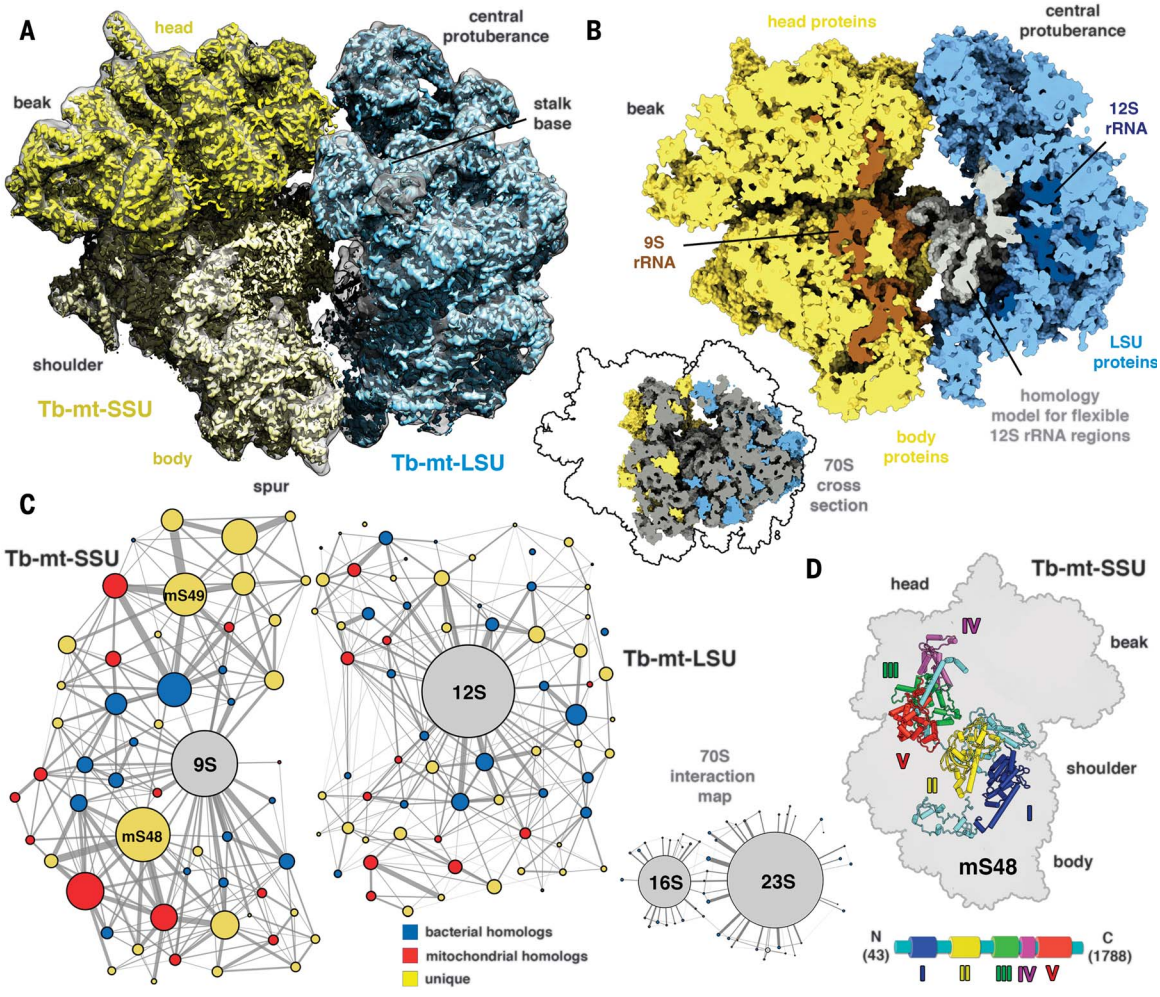

Fig. 1. Overview of the *T. brucei* mitoribosome. (**A**) Cryo-EM reconstruction of the complete trypanosomal mitoribosome shown in transparent gray together with the high-resolution maps of the large subunit (Tb-mt-LSU) in blue and the head and body of the small subunit (Tb-mt-SSU) in dark and bright yellow, respectively. (**B**) Cross section through the mitoribosome with the ribosomal proteins colored as in (A). The 12*S* rRNA homology model is shown in gray, and the atomic models of the 9*S* and the 12*S* rRNA are in brown and dark blue, respectively. Inset: A cross section through the bacterial 70*S* ribosome with the outline of the trypanosomal mitoribosome is shown for comparison. (**C**) Interaction network of all individual elements within the mitoribosome using the indicated color scheme. The size of nodes and thickness of edges correlate with the size of the surface of the individual elements and their interactions. A bacterial 70*S* interaction network (not to scale) is also shown. (**D**) Cartoon representation of mS48 with its individual domains.

the subunit interface, there are several less well-ordered disconnected densities that could not be assigned (fig. S4). The refined subunit structures were docked into the 7.8-Å map of the entire trypanosomal mitoribosome (Figs. 1 and 2 and figs. S2 and S3).

The overall structure of the trypanosomal mitoribosome

The trypanosomal mitoribosome has a diameter of ~385 Å, which makes this ribosome considerably larger and different in appearance than any other ribosomal complex described so far (Fig. 1) (*4*, *14*, *16*). Our structure disagrees with the cryo-EM map previously obtained for a related mitoribosome from *Leishmania tarentolae* (supplementary text) (*17*).

Both trypanosomal mitoribosomal subunits contain pronounced structural features that have not been observed in any other ribosomes: The small subunit harbors a massive beak region that increases the head size to 230 Å, making it almost as large as the body of the small subunit (Fig. 1, A and B). Notably, the small subunit with a calculated molecular weight of ~2.5 MDa is about three times larger than the canonical bacterial small subunit, thereby exceeding even the size of the "large" subunit of the trypanosomal mitoribosome. Also, the overall appearance of the large mitoribosomal subunit is unusual with its massive central protuberance (CP) and the L1 stalk formed entirely by ribosomal proteins.

Both 9*S* and 12*S* rRNAs are found at the core of the trypanosomal mitoribosome encased in a large and highly interconnected shell of mitoribosomal proteins (Fig. 1, B and C). A remarkable feature of the ribosomal protein shell is the size and domain organization of individual proteins such as mS48 or mS49. With a length of 1788 amino acids, mS48 folds into a multidomain protein, in which individual domains are connected by linker regions. This protein contacts numerous ribosomal proteins and extends from the body of the small subunit to the head while contacting the 9*S* rRNA only tangentially (Fig. 1, C and D). This suggests a central organizational role of mS48 in the formation of the protein network of the small subunit, which is in line with the growth defects observed when the protein is ablated by RNA interference (*18*). The second largest protein, mS49, is located in the head of the small subunit and establishes multiple protein-protein interactions that together bury a surface area of ~34,000 Å^2, an area comparable to the one between the bacterial small-subunit 16*S* rRNA and all 30*S* proteins (Fig. 1C and fig. S5) (*19*).

Apart from the 12*S* and 9*S* rRNA, we identified 127 mitoribosomal proteins, 70 in the large and 57 in the small subunit (Fig. 2 and table S2). Roughly half of the proteins are specific for trypanosomes and related species and, according to their molecular weight, were assigned as novel mitochondrial proteins mL67 to mL100 for the Tb-mt-LSU and mS48 to mS74 for the Tb-mt-SSU (table S2). Even among the conserved ribosomal proteins such as uS5m, uS9m, or bL17m, the homology is typically limited to the core domains, whereas the long extensions are specific for trypanosomes and together with the novel proteins amount to ~70% of the total protein mass of the trypanosomal mitoribosome

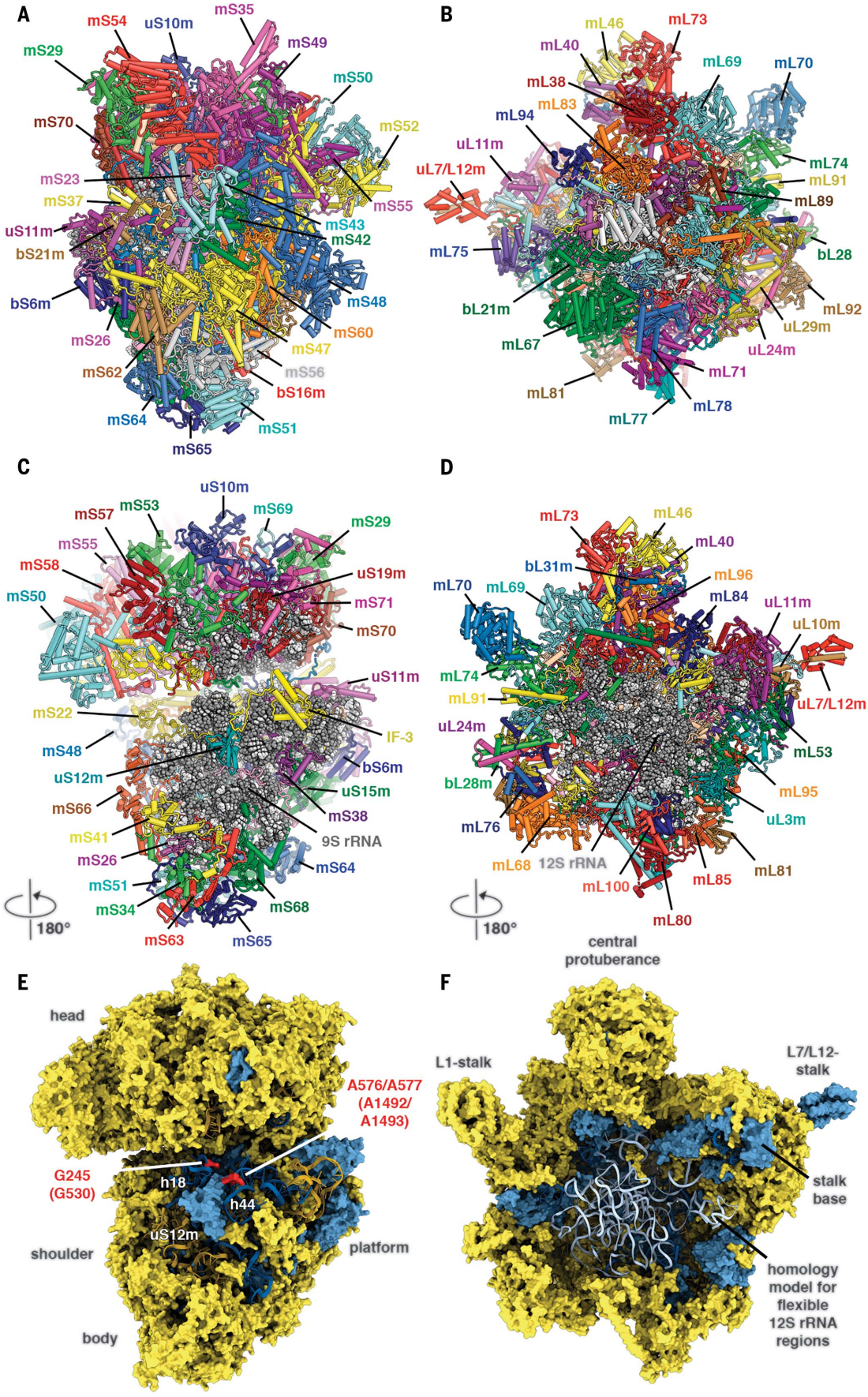

Fig. 2. Atomic models of the small and large mitoribosomal subunits and their universally conserved elements. (**A** to **D**) The individually colored mitoribosomal proteins are shown in cartoon and the rRNAs as gray spheres. The Tb-mt-SSU•IF3 complex (A and C) and the Tb-mt-LSU (B and D) are visualized from the solvent exposed side (A and B) and from the subunit interface (C and D). (**E** and **F**) View on the subunits as in (C) and (D) showing proteins as the surface and rRNAs as ribbons. Universally conserved elements are colored in blue, and the rest is in yellow. The decoding bases of the trypanosomal 9S rRNA (corresponding *E. coli* numbering in parentheses) are indicated in red.

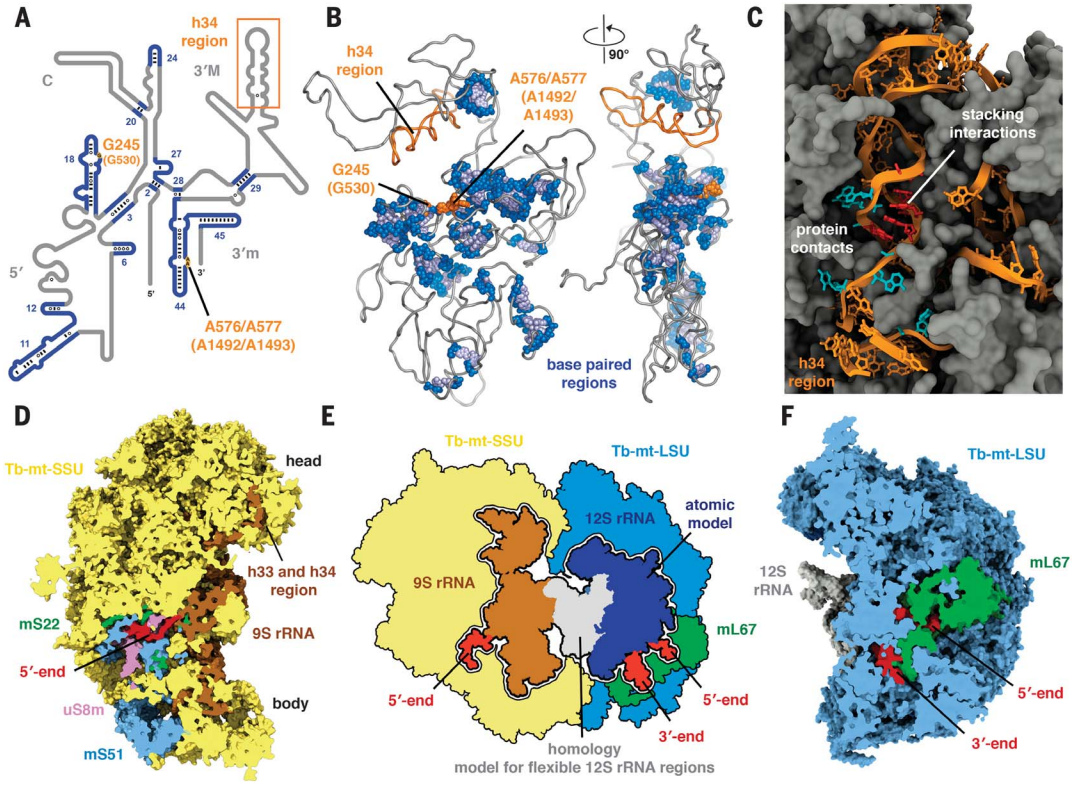

Fig. 3. Features of the 9*S* and 12*S* rRNA. (**A** and **B**) Secondary (A) and tertiary (B) structure of the 9S rRNA (gray) illustrating base pairing within residual helical regions (blue) together with the universal conserved decoding bases (orange). (**C**) Close-up view of the 9S rRNA helix h34 (orange cartoon) embedded into the Tb-mt-SSU head proteins (gray surface). (**D** to **F**) Cross sections of the Tb-mt-SSU (D) and Tb-mt-LSU (F) showing the anchoring of the 9S and 12S rRNA termini in the protein shell. The situation in the complete mitoribosome is visualized schematically in (E).

(figs. S6 and S7). Furthermore, trypanosomal mitoribosomal proteins are substantially larger than the bacterial homologs with a ~2.4 times increased median molecular weight. Consequently, the entire mitoribosome has a molecular weight of 4.5 MDa with an RNA/protein ratio of 1:6, which notably differs from the 2:1 ratio found in bacteria (*18*) and the 1:2 ratio found in mammalian mitochondria (*5*, *6*).

The structure of the *T. brucei* mitoribosome in which only a very small number of proteins and rRNA elements are preserved can help us to establish the minimal set of irreplaceable components of this machinery. For the large subunit, this includes the PTC with uL16m next to it and the exit tunnel region formed by uL4m, uL22m, and uL24m (Fig. 2F). Also, the L7/L12 stalk and its base are conserved, formed by the 12*S* rRNA helices H43 and H44 and the protein uL10m (Fig. 2F and fig. S8). The conserved core of the small subunit is even more reduced to the platform region formed by proteins bS6m, uS11m, uS15m, and bS21m (Fig. 2E), as well as the decoding center, where rRNA helices h18 and an extremely shortened h44 are located. These regions of the 9*S* rRNA contain the strictly conserved decoding residues G245 (G530 in *Escherichia coli*) and A576/A577 (A1492/A1493 in *E. coli*), with the sequence corresponding to the G530 loop being the longest conserved nucleotide pattern in the entire trypanosomal mitoribosome (Fig. 2E and fig. S9). The putative transfer RNA (tRNA) binding sites on the small mitoribosomal subunit are surrounded by a number of rRNA nucleotides that are not conserved at a sequence level but occupy equivalent positions in the structure to mediate tRNA interactions (fig. S10). The decoding center rRNA helices are held in place by protein uS12m in a similar manner as in other ribosomes. Trypanosomal uS12m may further play a role in the regulation of ribosome assembly considering that it is, unlike any other mitoribosomal protein, encoded as a cryptogene on the mitochondrial genome (*20*). Thus, its primary transcript is subject to extensive RNA editing, which is required to convert it into a translatable mRNA (fig. S11 and supplementary text) (*21*).

The rRNA of the trypanosomal mitoribosome

Mitochondrial rRNAs of trypanosomes represent markedly reduced versions of the typical rRNA as evidenced by comparing their secondary structure diagrams (figs. S8 and S9). The reduction is also apparent in the functionally important rRNA helices such as H38 in the large subunit and h18 or h44 in the small subunit (Fig. 3 and figs. S8 and S9). Compared to the rRNAs of the bacterial or mammalian mitoribosomal large subunits, many of the stem loop regions of the trypanosomal 12*S* rRNA have been shortened or removed (fig. S8). The changes in the 9*S* small-subunit rRNA are even more pronounced because not only were stem loops reduced but the secondary structure was also extensively remodeled (Fig. 3A and fig S9). In contrast to canonical rRNAs that adopt a compact fold dominated by base-paired double helical secondary structure elements, only ~20% of the 9*S* rRNA sequence is base paired (Fig. 3B). Accordingly, only 10 of 45 helices of the bacterial 16*S* rRNA are conserved in the 9*S* rRNA. In the head of the small subunit, almost all canonical rRNA helices of the 3′ major domain (h30 to h43) are absent or replaced by single-stranded segments of the 9*S* rRNA that are stabilized by either stacking interactions or through contacts with ribosomal proteins. For example, 9*S* rRNA residues 441 to 483 within the h34 region are twisted over a distance of 60 Å following an approximate helical path in the absence of any base pairs (Fig. 3C). Nevertheless, the helix h34 region still occupies the same location on the small subunit, possibly to mediate interactions with mitochondrial elongation factor EF-G1, whose bacterial homolog contacts the minor groove of h34 during tRNA translocation (*22*, *23*).

The interactions between ribosomal proteins and rRNA involve, in some cases, a very unusual topology. For example, the proteins mS53 and

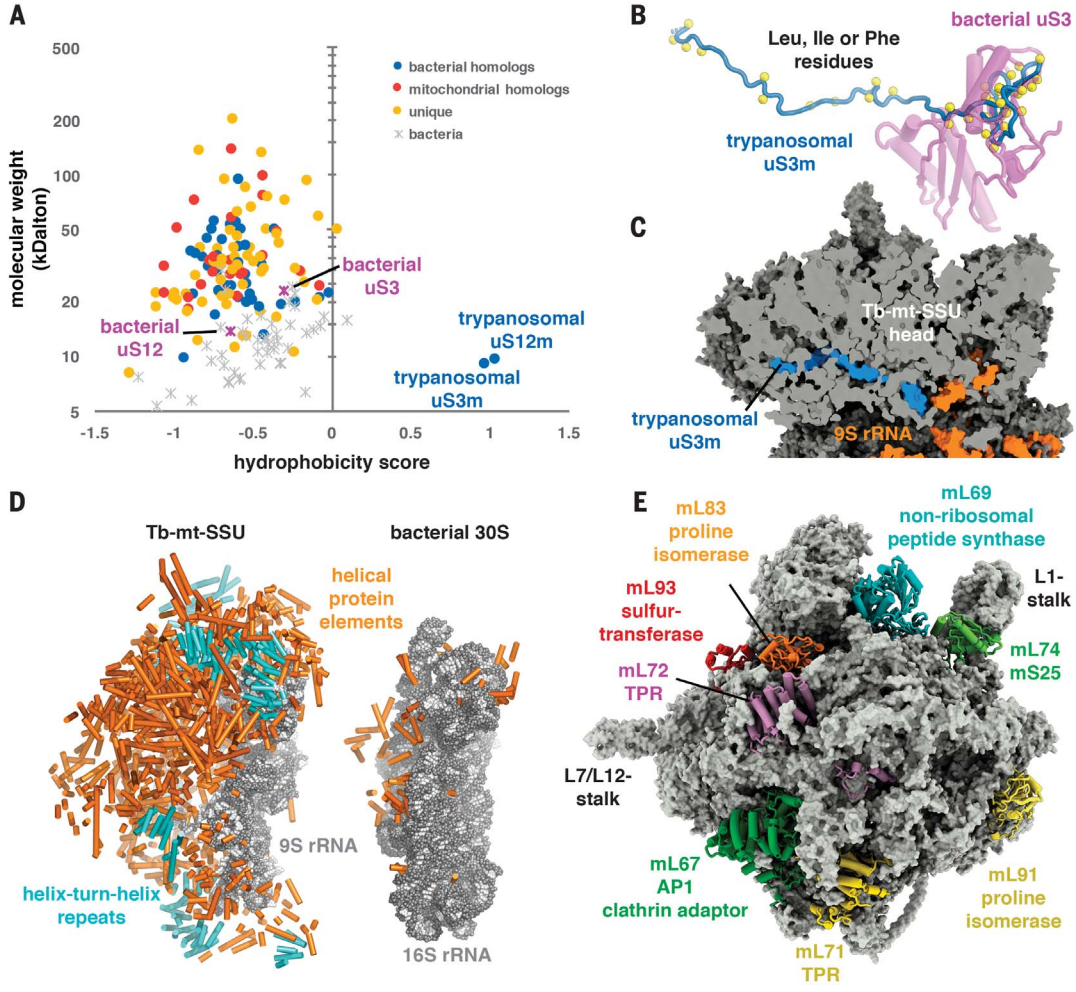

Fig. 4. Proteins of the trypanosomal mitoribosome. (**A**) The molecular weight (log scale) and hydrophobicity score (*31*) of all trypanosomal mitochondrial and bacterial ribosomal proteins (colors as indicated). (**B**) Cartoon representation of trypanosomal protein uS3m (blue) superimposed onto bacterial uS3 (violet). The hydrophobic residues of uS3m are shown as yellow spheres. (**C**) Surface representation of uS3m as an integral part of the Tb-mt-SSU head (proteins in gray and 9*S* rRNA in orange). (**D**) Side views onto the Tb-mt-SSU (left) and bacterial 30*S* small subunit (right) showing α helices of the ribosomal proteins (orange cartoons) and the rRNAs (gray spheres). Helical protein repeats are highlighted in cyan. (**E**) Numerous proteins (cartoon) that share structural homology to non-ribosomal proteins or enzymes are found in the Tb-mt-LSU (gray surface).

mS57 hook the rRNA to the head of the small subunit with their long N-terminal segments threaded through an rRNA loop in the h33 region (fig. S12), suggesting that folding of the 9*S* rRNA is coordinated with the folding and association of ribosomal proteins. This is also evidenced by the fact that the complementary sequences within many 9*S* rRNA regions, which are observed in a single-stranded conformation, would in theory allow the formation of helical structures (such as the equivalents to bacterial helices h7, h15, h22, or h30; fig. S9) (*7*–*9*). Therefore, it is likely that the binding of the 9*S* rRNA to the protein shell keeps it from adopting a secondary structure that would correspond to the lowest energy state predicted for this RNA based on sequence (*7*–*9*).

We observe that the rRNAs of both subunits are anchored in the protein shell (Fig. 3, D to F). This suggests that the massive protein shell represents a cradle that serves as a platform for the folding of the rRNA. The extended single-stranded 5′ end of the 9*S* rRNA is attached to mS51 and trypanosomal-specific elements of uS8m, uS22m, and mS47 (Fig. 3, D and E). In the case of the 12*S* rRNA, both the 5′ and 3′ ends are bound to trypanosomal-specific mL67, the largest Tb-mt-LSU protein (Fig. 3, E and F). These interactions effectively bring together the two ends of the 12*S* rRNA, which emulates the interactions observed in bacteria where the two ends of the 23*S* rRNA are circularized through base pairing of complementary sequences to generate helix H1, which is then processed during maturation (*24*).

Proteins of the trypanosomal mitoribosome

Within the trypanosomal mitoribosome, several functionally important regions of rRNA that play a role in interactions with the mRNA and tRNA substrates or undergo conformational changes during translation have been replaced by protein features. For example, the L1 stalk is solely formed by proteins bL9m, mL70, mL74, and mL91 that protrude away from the large subunit, thereby mimicking the features of the rRNA-based L1 stalk of other ribosomes (Fig. 2, B and D) (*18*). The canonical L1 stalk changes its position by up to 40 Å upon binding and release of tRNAs at the ribosomal E site (*25*). The preservation of structural features of this ribosomal element, although formed exclusively by ribosomal proteins instead of rRNA, suggests an indispensable functional role in interactions with the E-site tRNA and in modulating accompanying conformational changes (*26*).

The trypanosomal mitoribosomal CP is about three times the size of its bacterial counterpart (*18*). It is composed of bL31m, mL38, mL40, mL46, mL73, and mL96, thus representing the first ribosomal CP that is exclusively shaped by protein elements in the absence of any RNA element such as the 5*S* rRNA in bacteria (*18*), the CP-tRNA in the mammalian mitoribosome (*27*, *28*), or an extension of the large-subunit rRNA in yeast mitochondria (Fig. 2, B and D) (*29*). In terms of the protein composition, the trypanosomal CP is dominated by mitochondrial homologs, which suggests that this architectural landmark was already present in ancestral mitoribosomes before the eukaryotes branched into different groups (Fig. 2F and fig. S7).

With the switch to a protein-based architecture, we observe marked changes in the chemical properties of even the most conserved ribosomal proteins, with uS3m and uS12m being striking examples (Fig. 4A). Trypanosomal uS3m is surrounded exclusively by proteins instead of rRNA and shares structural homology with the CTD of bacterial uS3 (Fig. 4B). We identified

uS3m on the mitochondrial genome (table S2 and supplementary text), which is similar to yeast, where uS3m represents the only ribosomal protein encoded by the mitochondrial DNA (*30*). In contrast to typical ribosomal proteins that are rich in positively charged amino acids interacting with rRNA, trypanosomal uS3m is rich in hydrophobic amino acids (23% Ile, 13% Leu, and 13% Phe), resulting in an average hydrophobicity score comparable to membrane proteins (Fig. 4A) (*31*). Therefore, this protein appears to serve as a hydrophobic core in the protein shell (Fig. 4C). The extreme hydrophobic character of uS3m and uS12m may necessitate their cotranslational incorporation into the trypanosomal mitoribosome and may explain why both are encoded on the mitochondrial genome. However, this is unlikely to be the only source of evolutionary pressure to keep these genes on the mitochondrial genome because yeast uS3m has a hydrophilic character similar to bacterial protein (score of −0.786).

The structure of the trypanosomal mitoribosome provides insights into the large class of helical repeat proteins containing penta/tetratricopeptide repeat (P/TPR), HEAT, or ARM motifs (Fig. 4D) (*32*, *33*). The group of P/TPR-containing proteins are characterized as single-stranded RNA binding proteins, frequently found in the chloroplasts and mitochondria. P/TPR proteins were extensively characterized by sequence analysis and biochemical experiments (*33*) and suggested to be part of the trypanosomal mitoribosome (*34*, *35*). Our results reveal the structures and the network of interactions of six P/TPR-containing mitoribosomal proteins (table S2). All of these proteins mediate protein-protein interactions, whereas only some have peripheral contact to rRNA. Presumably, these P/TPR-containing proteins had originally been recruited to single-stranded rRNA segments and maintained their position as integral architectural elements, whereas the surrounding rRNA was reduced (fig. S13 and supplementary text). In general, we observe that the trypanosomal-specific proteins and protein extensions harbor a disproportionally large fraction of α-helical secondary structure elements, many arising from superhelical structures of repetitive helix-turn-helix motifs that architecturally substitute for the reduced rRNA. For the small subunit, the ratio of α helix versus β sheet content is 7.5:1 in trypanosomal mitoribosomes, whereas it is 2:1 in bacterial ribosomes (Fig. 4D).

Many solvent-exposed proteins of the trypanosomal mitoribosome are structurally homologous to nonribosomal proteins or enzymes. The folds of the AP1 clathrin adaptor (mL67), proline isomerase (mL91), sulfur transferase (mL93), and nonribosomal peptide synthase (mL69) are found in the large subunit and those of thiosulfate sulfurtransferase (mS67) and A-kinase anchoring protein (mS64) in the small subunit (Fig. 4E and table S2). However, these proteins with homology to enzymes contain

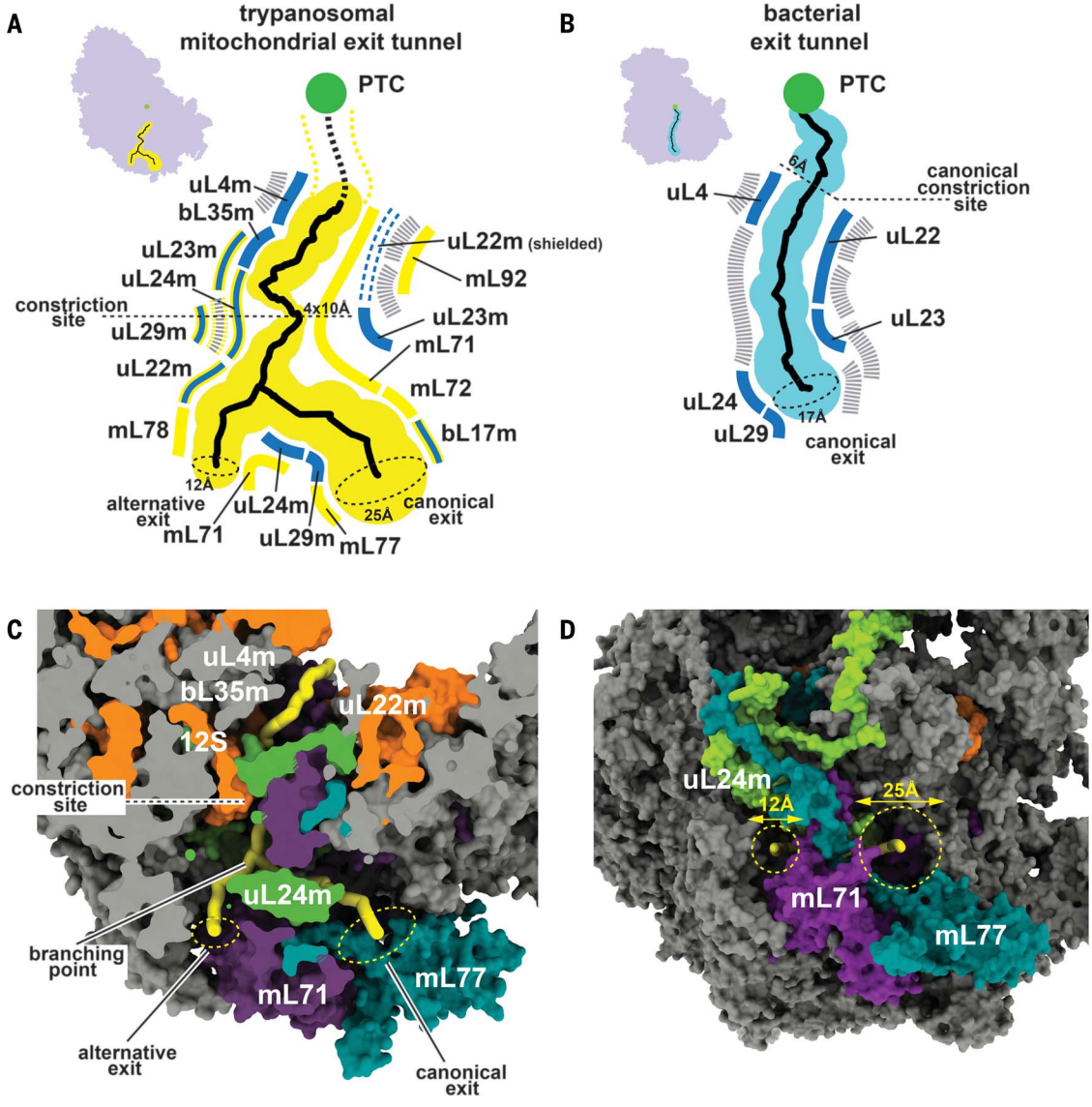

Fig. 5. The trypanosomal mitoribosomal exit tunnel. (**A** and **B**) Schematics of the architecture of the exit tunnel emerging from the PTC (green sphere) found in trypanosomal mitochondria (A) and bacteria (B). The exit tunnels are surrounded by conserved protein (blue lines) and rRNA elements (gray dashed lines). Trypanosomal-specific elements are colored in yellow (proteins), yellow-blue (protein extensions), and gray-yellow (rRNA segment at the tunnel constriction). (**C** and **D**) Surface representation of the tunnel path and the two exit sites (yellow) in a cross section (C) or from the exterior (D), with proteins in gray and the rRNA in orange. The branching of the exit tunnel is mediated by uL24m (green), mL71 (purple), and mL77 (dark cyan).

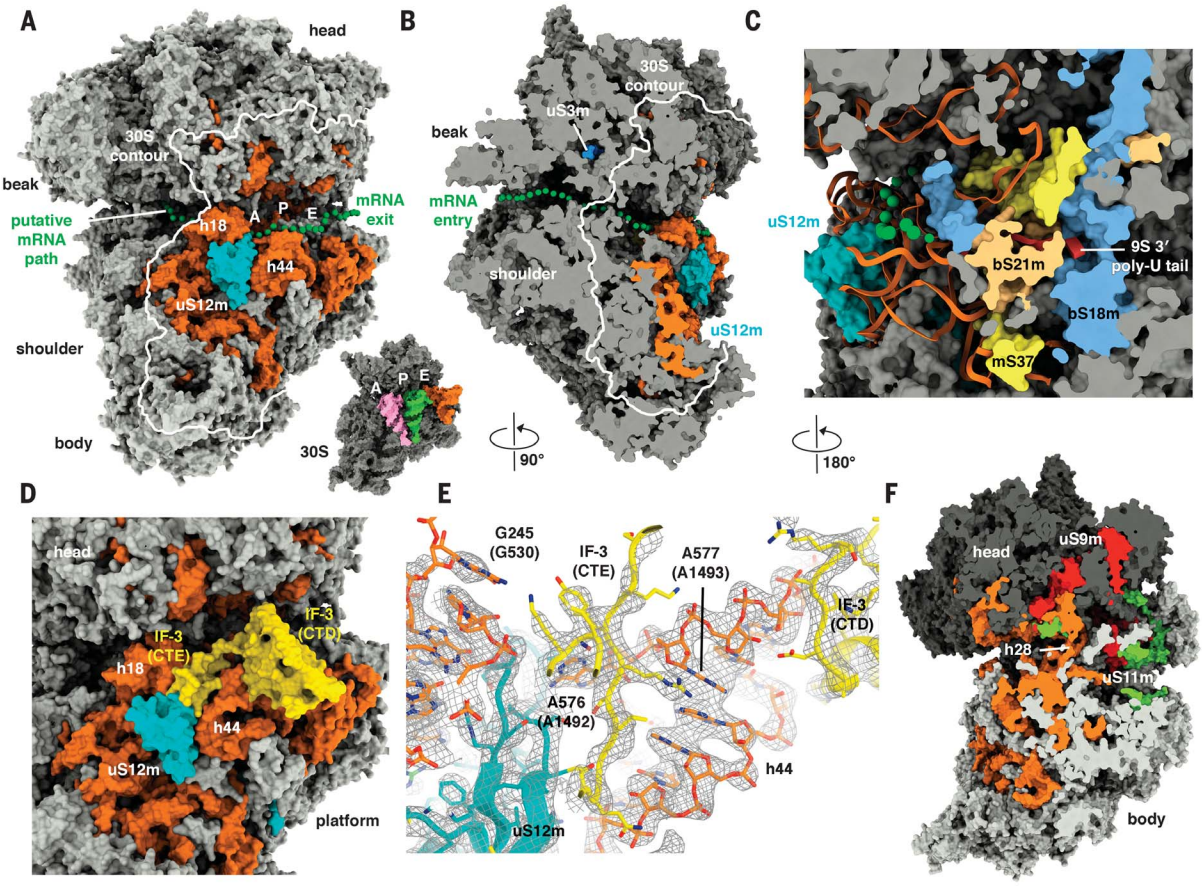

Fig. 6. The small trypanosomal mitoribosomal subunit in complex with IF-3. (**A** to **C**) The putative mRNA path (depicted by green spheres) in the Tb-mt-SSU is shown from the subunit interface and in cross sections through the shoulder (B) or the platform regions (C). Proteins are shown in gray, the 9S rRNA in orange, and uS12m in cyan, together with a contour of the bacterial 30S (white outline). The bacterial 30S subunit in complex with A-, P-, and E-site tRNAs is shown in the inset. Trypanosomal proteins bS18m (blue), bS21m (sand), and mS37 (yellow) partially shield the 3′ poly-U tail (red) from the mRNA path. (**D** and **E**) Interaction of the C-terminal extension (CTE) of the CTD of IF-3 (yellow) with h44 at the decoding center (orange) shown in surface (D) and cartoon (E) representation together with experimental cryo-EM density (gray). (**F**) Cross section of the Tb-mt-SSU showing the head (dark gray) and body (light gray) connection formed by the 9S rRNA (orange) and proteins uS9m (red) and uS11m (green).

mutations of catalytically important amino acids in their active sites, suggesting that they lost their enzymatic activity and rather play an architectural role in the trypanosomal mitoribosome. Furthermore, we identified several bound cofactors that typically participate in enzymatic reactions; whereas in the trypanosomal mitoribosome, they apparently play a purely structural role (fig. S14 and supplementary text). These include nicotinamide adenine dinucleotide that bridges uL4m, uL15m, and mL64, a guanosine triphosphate bound to mS29, and a nucleoside triphosphate (NTP) bound to a positively charged binding pocket created between the helical repeats of mS53, mS57, and the 9*S* rRNA (figs. S12 and S14). Presumably, this NTP represents a relic of the 9*S* rRNA reduction that occurred most prominently in the head region of the Tb-mt-SSU (Fig. 3A).

The remodeled exit tunnel of the large subunit

Because of the recruitment of specific proteins or protein extensions to the trypanosomal mitoribosome, the tunnel and the exit region have evolved unique molecular features. We computationally analyzed the tunnel width to reveal a putative path of the nascent polypeptide (*36*). The trypanosomal tunnel wall is formed mostly by proteins rather than rRNA. In addition to the core folds of conserved proteins uL4m, uL23m, uL24m, and uL29m that still contribute to shaping of the exit tunnel, the tunnel wall is lined by numerous trypanosomal-specific proteins or protein extensions (Fig. 5 and fig. S15). The conserved β sheet of uL22m that usually lines the tunnel is covered by the N-terminal extension of mL71 that changes the path of the tunnel. Further down, mL71 together with trypanosomal-specific elements of uL24m and of the 12*S* rRNA narrows the tunnel elliptically to ~10 × 4 Å^2, which would only allow the passage of an unfolded protein. Notably, the tunnel in yeast mitochondria also contains a constriction in this region, which includes uL22m and uL24m, that has been suggested to have a regulatory role (*28*).

Because of trypanosomal-specific elements in uL24m, mL71, and mL77, the tunnel branches, resulting in a smaller exit with a diameter of ~12 Å and a larger exit with a diameter of ~25 Å (Fig. 5A). The larger tunnel exit points into a similar direction as the canonical bacterial exit, whereas the positioning of the alternative smaller exit is close to the one found in yeast mitoribosomes (*28*). This observation provides for an interesting possibility that the canonical exit is used for the synthesis and cotranslational insertion of membrane proteins, whereas the smaller alternative exit may be used for the synthesis of matrix proteins such as uS3m and uS12m without the need to detach the ribosome from the membrane.

The mRNA path of the small subunit

Modeling of the bacterial mRNA based on superposition of the few conserved protein cores and rRNA elements of the decoding site reveals the location of the mRNA channel, with its entrance and exit regions in the small subunit (Fig. 6A) (*37*). In trypanosomes, uS5m represents the only conserved element facing the mRNA at the entry site, as uS4m does not

exist and uS3m is buried under the trypanosomal-specific protein mS59 and an extension of uS10m. Because of the large beak and shoulder regions, the canonical mRNA entry path below the beak is extended by ~150 Å (Fig. 6B).

The mRNA exit region at the Tb-mt-SSU platform is close to the location of the 3′ end of the 9*S* rRNA, which harbors seven uracil residues that are added posttranscriptionally (*38*). The 3′ end of the 9*S* rRNA occupies a similar position relative to the mRNA channel as the anti–Shine-Dalgarno sequence at the 3′ end of the bacterial 16*S* rRNA (Fig. 6C). Nevertheless, the poly-U tail is sequestered by bS18m, bS21m, and mS37 and is therefore not available for base-pairing interactions with mRNAs.

The small subunit in complex with mitochondrial IF-3

The cryo-EM reconstruction of the isolated small subunit reveals that it is in complex with mitochondrial IF-3, whose CTD can be seen bound to the top of the shortened helix h44 (Fig. 6D). This position is similar to observed for bacterial IF-3 (*39*) and suggests that the Tb-mt-SSU•IF-3 complex represents a post-recycling/preinitiation state that precedes mRNA and initiator tRNA binding during translation initiation.

Currently, the role of mitochondrial IF-3 is not well understood, and our Tb-mt-SSU•IF-3 complex indicates a possible mechanistic role for its C-terminal extension during initiation in trypanosomes. This region of the mitochondrial IF-3 interacts with the decoding center and stabilizes A576 (A1492 in *E. coli*) in a flipped-out position, pointing away from the putative mRNA channel to allow mRNA positioning (Fig. 6E). This function is similar to what was observed for the bacterial IF-1 that interacts with the decoding center and stabilizes bases A1492 and A1493 in a flipped-out conformation (*39*, *40*). This observation explains how the C-terminal extension of trypanosomal mitochondrial IF-3 can compensate for the missing IF-1, which is universally absent in mitochondria (*41*) but is an essential initiation factor in bacteria and yeast (*42*, *43*).

Although the small subunit changed shape due to additions of many new proteins, there is still a well-defined separation between the head and the body to allow for the rotation that is mechanistically important during initiation and for repositioning of tRNAs during translation elongation (Fig. 6F) (*44*). Nevertheless, it is likely that the flexibility between the head and the body is reduced in the trypanosomal small subunit because the two parts are covalently connected not only through rRNA, as is typically the case, but also through several proteins (Fig. 6E). As a consequence, the comparison between the free and complexed small subunits reveals head to body tilting instead of the canonical twisting rotation (fig. S16).

Conclusions

Our results define the composition and the structure of the extremely remodeled mitoribosome of trypanosomes. Its unusual architecture markedly deviates from the structures of all other ribosomes and allows us to better define the universally conserved core of the ribosome that is responsible for the most basic ribosomal functions. We also observe that the architectural role of the rRNA during ribosomal assembly has been taken over by proteins. This implies that ribosomal biogenesis is unlikely to proceed through initial folding of rRNA helices that coalesce into an rRNA dominated tertiary structure with the help of ribosomal proteins and maturation factors. Instead, the trypanosomal ribosome is more likely to assemble through binding of the unfolded rRNA to the preformed elements of the protein shell. The structure also extends our understanding of mitochondrial translation and of the role of mitochondrial IF-3 in particular. Last, because some trypanosomes are human pathogens, this unique structure may be helpful for developing antibiotics to treat sleeping sickness, Chagas disease, or Leishmaniasis.

Materials and methods summary

Purification of the T. brucei *mitoribosome and cryo-EM analysis*

For the affinity purification of a *T. brucei* mitoribosomal sample, we introduced PTP affinity tags at the C-termini of different mitoribosomal proteins (*45*). Such affinity purified complexes were analyzed by electron microscopy and mass spectrometry (*15*).

An aliquot of purified sample was loaded on a holey carbon copper grid that was pre-coated with a thin carbon film. The grid was subsequently plunge frozen using an FEI Vitrobot Mark IV. Individual cryo-EM data sets obtained from either LSU-tagged or SSU-tagged mitoribosomes were collected using a FEI Titan Krios cryo-transmission electron microscope (TEM) equipped with a FEI Falcon III direct electron detector.

Initial references for the Tb-mt-SSU and Tb-mt-LSU were calculated ab initio with EMAN (*46*) using subsets of characteristic 2D class averages from negative stain EM data sets that were either depleted (Tb-mt-SSU) or enriched (Tb-mt-LSU) under dissociating conditions in a mitoribosomal sample carrying a LSU-tag (fig. S2A). These initial models were used for the first steps of particle picking and initial 3D alignments and iteratively improved during the 3D classification process. The structures were refined using masks for the entire Tb-mt-SSU•IF-3, the Tb-mt-SSU head or the Tb-mt-SSU•IF-3 body, the Tb-mt-LSU or without a mask in the case of the complete trypanosomal mitoribosome (fig. S2B). Final data sets included 101,308 particle images for the Tb-mt-SSU head, 31,911 particle images for the Tb-mt-SSU•IF-3 body, 31,619 particle images for the Tb-mt-LSU and 7141 particle images for the complete trypanosomal mitoribosome. Using the FSC = 0.143 criterion, these reconstructions were resolved at 3.1 Å for the Tb-mt-SSU head, 3.3 Å for the Tb-mt-SSU•IF-3 body, 3.4 Å for the Tb-mt-LSU and 7.8 Å for the complete trypanosomal mitoribosome (fig. S2C).

Structure building and model refinement

The atomic model of the trypanosomal ribosome was built into the high-resolution maps of the Tb-mt-SSU head, Tb-mt-SSU•IF-3 body and the Tb-mt-LSU (fig. S3 and table S1) using *Coot* (*47*) and O (*48*, *49*). Only the core areas of the conserved ribosomal homologs were found to share homology with the mammalian mitoribosome or the bacterial ribosome (*5*, *6*, *19*). For most proteins, their fold and identity was deduced from the experimental cryo-EM density by predicting their amino acid side chains according to the density features and their chemical environment followed by sequence homology search.

The 12*S* and 16*S* rRNAs from the mammalian mitoribosome (*5*, *6*) were docked into the structurally conserved core areas of trypanosomal rRNA and served as initial models to establish the correct registry. Additional elements were added to these rRNA models in agreement with the remaining 9*S* and 12*S* rRNA sequences. Whereas for the 9*S* rRNA a complete atomic model was built, we were able to interpret about 50% of the 12*S* rRNA in well-ordered areas. To display the missing parts of the 12*S* rRNA that included regions around the PTC (Figs. 1 to 3), we generated a homology model based on the mammalian mitoribosomal 16*S* rRNA using the predicted secondary structure as a guide (*9*). These parts are not included in the final atomic model.

The atomic models of the Tb-mt-SSU head, Tb-mt-SSU•IF-3 body, the complete Tb-mt-SSU•IF-3 and the Tb-mt-LSU were refined with PHENIX (*50*, *51*) using a combination of secondary structure restrained real and reciprocal space refinement. F_{obs}–F_{calc} difference Fourier maps were used to detect and eliminate errors and to identify missing co-factors and additional ions. Table S1 summarizes the refinement and provides model statistics. For the model of the complete mitoribosome, the high-resolution coordinates were docked into the 7.8 Å cryo-EM map of the complete trypanosomal mitoribosome.

REFERENCES AND NOTES

1. T. M. Schmeing, V. Ramakrishnan, What recent ribosome structures have revealed about the mechanism of translation. *Nature* **461**, 1234–1242 (2009). doi: 10.1038/nature08403 pmid: 19838167
2. R. R. Gutell, B. Weiser, C. R. Woese, H. F. Noller, Comparative anatomy of 16-S-like ribosomal RNA. *Prog. Nucleic Acid Res. Mol. Biol.* **32**, 155–216 (1985). doi: 10.1016/S0079-6603(08)60348-7 pmid: 3911275
3. C. R. Woese, G. E. Fox, Phylogenetic structure of the prokaryotic domain: The primary kingdoms. *Proc. Natl. Acad. Sci. U.S.A.* **74**, 5088–5090 (1977). doi: 10.1073/pnas.74.11.5088 pmid: 270744
4. S. Melnikov *et al.*, One core, two shells: Bacterial and eukaryotic ribosomes. *Nat. Struct. Mol. Biol.* **19**, 560–567 (2012). doi: 10.1038/nsmb.2313; pmid: 22664983
5. A. Amunts, A. Brown, J. Toots, S. H. W. Scheres, V. Ramakrishnan, The structure of the human mitochondrial ribosome. *Science* **348**, 95–98 (2015). doi: 10.1126/science.aaa1193 pmid: 25838379

6. B. J. Greber *et al*., The complete structure of the 55S mammalian mitochondrial ribosome. *Science* **348**, 303–308 (2015). doi: 10.1126/science.aaa3872; pmid: 25837512
7. V. F. de la Cruz, J. A. Lake, A. M. Simpson, L. Simpson, A minimal ribosomal RNA: Sequence and secondary structure of the 9S kinetoplast ribosomal RNA from Leishmania tarentolae. *Proc. Natl. Acad. Sci. U.S.A.* **82**, 1401–1405 (1985). doi: 10.1073/pnas.82.5.1401; pmid: 3856267
8. I. C. Eperon, J. W. Janssen, J. H. Hoeijmakers, P. Borst, The major transcripts of the kinetoplast DNA of Trypanosoma brucei are very small ribosomal RNAs. *Nucleic Acids Res.* **11**, 105–125 (1983). doi: 10.1093/nar/11.1.105; pmid: 6306559
9. P. Sloof *et al*., Further characterization of the extremely small mitochondrial ribosomal RNAs from trypanosomes: A detailed comparison of the 9S and 12S RNAs from Crithidia fasciculata and Trypanosoma brucei with rRNAs from other organisms. *Nucleic Acids Res.* **13**, 4171–4190 (1985). doi: 10.1093/nar/13.11.4171; pmid: 2409531
10. D. A. Maslov *et al*., Isolation and characterization of mitochondrial ribosomes and ribosomal subunits from *Leishmania tarentolae*. *Mol. Biochem. Parasitol.* **148**, 69–78 (2006). doi: 10.1016/j.molbiopara.2006.02.021; pmid: 16600399
11. H. H. Shu, H. U. Göringer, Trypanosoma brucei mitochondrial ribonucleoprotein complexes which contain 12S and 9S ribosomal RNAs. *Parasitology* **116**, 157–164 (1998). doi: 10.1017/S0031182097002023; pmid: 9509025
12. A. Zíková *et al*., *Trypanosoma brucei* mitochondrial ribosomes: Affinity purification and component identification by mass spectrometry. *Mol. Cell. Proteomics* **7**, 1286–1296 (2008). doi: 10.1074/mcp.M700490-MCP200; pmid: 18364347
13. N. Desai, A. Brown, A. Amunts, V. Ramakrishnan, The structure of the yeast mitochondrial ribosome. *Science* **355**, 528–531 (2017). doi: 10.1126/science.aal2415; pmid: 28154081
14. S. Klinge, F. Voigts-Hoffmann, M. Leibundgut, N. Ban, Atomic structures of the eukaryotic ribosome. *Trends Biochem. Sci.* **37**, 189–198 (2012). doi: 10.1016/j.tibs.2012.02.007; pmid: 22436288
15. Materials and methods are available as supplementary materials.
16. P. Bieri, B. J. Greber, N. Ban, High-resolution structures of mitochondrial ribosomes and their functional implications. *Curr. Opin. Struct. Biol.* **49**, 44–53 (2018). doi: 10.1016/j.sbi.2017.12.009; pmid: 29348055
17. M. R. Sharma, T. M. Booth, L. Simpson, D. A. Maslov, R. K. Agrawal, Structure of a mitochondrial ribosome with minimal RNA. *Proc. Natl. Acad. Sci. U.S.A.* **106**, 9637–9642 (2009). doi: 10.1073/pnas.0901631106; pmid: 19497863
18. D.-E. Mbang-Benet *et al*., RNA interference screen reveals a high proportion of mitochondrial proteins essential for correct cell cycle progress in *Trypanosoma brucei*. *BMC Genomics* **16**, 297 (2015). doi: 10.1186/s12864-015-1505-5 pmid: 25888089
19. M. Selmer *et al*., Structure of the 70S ribosome complexed with mRNA and tRNA. *Science* **313**, 1935–1942 (2006). doi: 10.1126/science.1131127; pmid: 16959973
20. C. Marchal, N. Ismaïli, E. Pays, A ribosomal S12-like gene of *Trypanosoma brucei*. *Mol. Biochem. Parasitol.* **57**, 331–334 (1993). doi: 10.1016/0166-6851(93)90208-F; pmid: 8433721
21. I. Aphasizheva, D. A. Maslov, R. Aphasizhev, Kinetoplast DNA-encoded ribosomal protein S12: A possible functional link between mitochondrial RNA editing and translation in Trypanosoma brucei. *RNA Biol.* **10**, 1679–1688 (2013). doi: 10.4161/rna.26733; pmid: 24270388
22. A. B. Matassova, M. V. Rodnina, W. Wintermeyer, Elongation factor G-induced structural change in helix 34 of 16S rRNA related to translocation on the ribosome. *RNA* **7**, 1879–1885 (2001). pmid: 11780642
23. A. H. Ratje *et al*., Head swivel on the ribosome facilitates translocation by means of intra-subunit tRNA hybrid sites. *Nature* **468**, 713–716 (2010). doi: 10.1038/nature09547; pmid: 21124459
24. Ü. Allas, A. Liiv, J. Remme, Functional interaction between RNase III and the Escherichia coli ribosome. *BMC Mol. Biol.* **4**, 8 (2003). doi: 10.1186/1471-2199-4-8; pmid: 12814522
25. S. Mohan, H. F. Noller, Recurring RNA structural motifs underlie the mechanics of L1 stalk movement. *Nat. Commun.* **8**, 14285 (2017). doi: 10.1038/ncomms14285; pmid: 28176782
26. L. G. Trabuco *et al*., The role of L1 stalk–tRNA interaction in the ribosome elongation cycle. *J. Mol. Biol.* **402**, 741–760 (2010). doi: 10.1016/j.jmb.2010.07.056; pmid: 20691699
27. A. Brown *et al*., Structure of the large ribosomal subunit from human mitochondria. *Science* **346**, 718–722 (2014). doi: 10.1126/science.1258026; pmid: 25278503
28. B. J. Greber *et al*., The complete structure of the large subunit of the mammalian mitochondrial ribosome. *Nature* **515**, 283–286 (2014). doi: 10.1038/nature13895; pmid: 25271403
29. A. Amunts *et al*., Structure of the yeast mitochondrial large ribosomal subunit. *Science* **343**, 1485–1489 (2014). doi: 10.1126/science.1249410; pmid: 24675956
30. G. S. Groot, T. L. Mason, N. Van Harten-Loosbroek, Var_1 is associated with the small ribosomal subunit of mitochondrial ribosomes in yeast. *Mol. Gen. Genet.* **174**, 339–342 (1979). doi: 10.1007/BF00267808; pmid: 384172
31. J. Kyte, R. F. Doolittle, A simple method for displaying the hydropathic character of a protein. *J. Mol. Biol.* **157**, 105–132 (1982). doi: 10.1016/0022-2836(82)90515-0; pmid: 7108955
32. M. A. Andrade, C. Petosa, S. I. O'Donoghue, C. W. Müller, P. Bork, Comparison of ARM and HEAT protein repeats. *J. Mol. Biol.* **309**, 1–18 (2001). doi: 10.1006/jmbi.2001.4624; pmid: 11491282
33. S. Manna, An overview of pentatricopeptide repeat proteins and their applications. *Biochimie* **113**, 93–99 (2015). doi: 10.1016/j.biochi.2015.04.004; pmid: 25882680
34. I. Aphasizheva *et al*., Ribosome-associated pentatricopeptide repeat proteins function as translational activators in mitochondria of trypanosomes. *Mol. Microbiol.* **99**, 1043–1058 (2016). doi: 10.1111/mmi.13287; pmid: 26713541
35. M. Pusnik, I. Small, L. K. Read, T. Fabbro, A. Schneider, Pentatricopeptide repeat proteins in *Trypanosoma brucei* function in mitochondrial ribosomes. *Mol. Cell. Biol.* **27**, 6876–6888 (2007). doi: 10.1128/MCB.00708-07; pmid: 17646387
36. K. Berka *et al*., MOLE*online* 2.0: Interactive web-based analysis of biomacromolecular channels. *Nucleic Acids Res.* **40**, W222–W227 (2012). doi: 10.1093/nar/gks363; pmid: 22553366
37. L. B. Jenner, N. Demeshkina, G. Yusupova, M. Yusupov, Structural aspects of messenger RNA reading frame maintenance by the ribosome. *Nat. Struct. Mol. Biol.* **17**, 555–560 (2010). doi: 10.1038/nsmb.1790; pmid: 20400952
38. B. K. Adler, M. E. Harris, K. I. Bertrand, S. L. Hajduk, Modification of Trypanosoma brucei mitochondrial rRNA by posttranscriptional 3′ polyuridine tail formation. *Mol. Cell. Biol.* **11**, 5878–5884 (1991). doi: 10.1128/MCB.11.12.5878; pmid: 1719373
39. T. Hussain, J. L. Llácer, B. T. Wimberly, J. S. Kieft, V. Ramakrishnan, Large-scale movements of IF3 and tRNA during bacterial translation initiation. *Cell* **167**, 133–144.e13 (2016). doi: 10.1016/j.cell.2016.08.074; pmid: 27662086
40. A. P. Carter *et al*., Crystal structure of an initiation factor bound to the 30S ribosomal subunit. *Science* **291**, 498–501 (2001). doi: 10.1126/science.1057766; pmid: 11228145
41. G. C. Atkinson *et al*., Evolutionary and genetic analyses of mitochondrial translation initiation factors identify the missing mitochondrial IF3 in *S. cerevisiae*. *Nucleic Acids Res.* **40**, 6122–6134 (2012). doi: 10.1093/nar/gks272; pmid: 22457064
42. H. S. Cummings, J. W. Hershey, Translation initiation factor IF1 is essential for cell viability in Escherichia coli. *J. Bacteriol.* **176**, 198–205 (1994). doi: 10.1128/jb.176.1.198-205.1994; pmid: 8282696
43. C.-L. Wei, M. Kainuma, J. W. B. Hershey, Characterization of yeast translation initiation factor 1A and cloning of its essential gene. *J. Biol. Chem.* **270**, 22788–22794 (1995). doi: 10.1074/jbc.270.39.22788; pmid: 7559407
44. S. Mohan, J. P. Donohue, H. F. Noller, Molecular mechanics of 30S subunit head rotation. *Proc. Natl. Acad. Sci. U.S.A.* **111**, 13325–13330 (2014). doi: 10.1073/pnas.1413731111; pmid: 25187561
45. B. Schimanski, T. N. Nguyen, A. Günzl, Highly efficient tandem affinity purification of trypanosome protein complexes based on a novel epitope combination. *Eukaryot. Cell* **4**, 1942–1950 (2005). doi: 10.1128/EC.4.11.1942-1950.2005; pmid: 16278461
46. S. J. Ludtke, P. R. Baldwin, W. Chiu, EMAN: Semiautomated software for high-resolution single-particle reconstructions. *J. Struct. Biol.* **128**, 82–97 (1999). doi: 10.1006/jsbi.1999.4174; pmid: 10600563
47. P. Emsley, B. Lohkamp, W. G. Scott, K. Cowtan, Features and development of *Coot*. *Acta Crystallogr. D Biol. Crystallogr.* **66**, 486–501 (2010). doi: 10.1107/S0907444910007493; pmid: 20383002
48. T. A. Jones, Interactive electron-density map interpretation: From *INTER* to *O*. *Acta Crystallogr. D Biol. Crystallogr.* **60**, 2115–2125 (2004). doi: 10.1107/S0907444904023509; pmid: 15572764
49. T. A. Jones, J. Y. Zou, S. W. Cowan, M. Kjeldgaard, Improved methods for building protein models in electron density maps and the location of errors in these models. *Acta Crystallogr. A* **47**, 110–119 (1991). doi: 10.1107/S0108767390010224; pmid: 2025413
50. P. D. Adams *et al*., *PHENIX*: A comprehensive Python-based system for macromolecular structure solution. *Acta Crystallogr. D Biol. Crystallogr.* **66**, 213–221 (2010). doi: 10.1107/S0907444909052925; pmid: 20124702
51. P. V. Afonine *et al*., Towards automated crystallographic structure refinement with *phenix.refine*. *Acta Crystallogr. D Biol. Crystallogr.* **68**, 352–367 (2012). doi: 10.1107/S0907444912001308; pmid: 22505256

ACKNOWLEDGMENTS

We thank E. Kummer, A. Scaiola, A. Jomaa, C. H. S. Aylett, B. Schimanski, and C. M. T. Spahn for support and discussions. Cryo-EM data were collected at the Scientific Center for Optical and Electron Microscopy (ScopeM) of ETH Zurich, and we thank P. Tittmann (ScopeM) for the support. A.L. would like to thank R. Aebersold for access to instrumentation and infrastructure. The Orbitrap Elite mass spectrometer was funded by an ETH Scientific Equipment grant. The cryo-EM data were processed on the Euler computing cluster of the Swiss National Supercomputing Centre (CSCS). **Funding:** This work was supported by the Swiss National Science Foundation (SNSF) and the National Center of Excellence in Research (NCCR) RNA and disease program of the SNSF. D.J.F.R. was supported by a FEBS long-term fellowship. **Author contributions:** D.J.F.R., M.N., A.S., and N.B. designed the experiment. M.N. and E.K.H. cloned the *T. brucei* strains. M.N., E.K.H., D.J.F.R., and C.P. purified the mitochondrial ribosomes. A.L. designed and performed the mass spectrometry analysis. D.J.F.R. and C.P. prepared cryo-EM grids. D.J.F.R. and D.B. acquired the cryo-EM data. D.J.F.R. and D.B. calculated the cryo-EM reconstructions. D.J.F.R., M.L., P.B., D.B., and N.B. interpreted the structures. D.J.F.R., M.L., P.B., and N.B. wrote the manuscript. All authors contributed to the final version of the paper. **Competing interests:** The authors declare no competing interests. **Data and materials availability:** The cryo-EM maps and PDB coordinates have been deposited in the Electron Microscopy Databank and PDB database, respectively. These entries include the complex of the complete *T. brucei* mitoribosome (EMD-0229 and PDB-6HIV), the complete Tb-mt-SSU•IF-3 (EMD-0230 and PDB-6HIW), the Tb-mt-LSU (EMD-0231 and PDB-6HIX), the Tb-mt-SSU•IF-3 body (EMD-0232 and PDB-6HIY), and the Tb-mt-SSU head (EMD-0233 and PDB-6HIZ). A PyMOL script for display of the complete trypanosomal mitoribosome is available from the Ban Lab website (www.bangroup.ethz.ch/).

SUPPLEMENTARY MATERIALS

www.sciencemag.org/content/362/6413/eaau7735/suppl/DC1
Materials and Methods
Supplementary Text
Figs. S1 to S16
Tables S1 and S2
References (*52*–*93*)
Data S1

13 July 2018; accepted 3 September 2018
Published online 13 September 2018
10.1126/science.aau7735

Evolutionary shift toward protein-based architecture in trypanosomal mitochondrial ribosomes

David J. F. Ramrath, Moritz Niemann, Marc Leibundgut, Philipp Bieri, Cline Prange, Elke K. Horn, Alexander Leitner, Daniel Boehringer, Andr Schneider, and Nenad Ban

Science, **362** (6413), eaau7735.
DOI: 10.1126/science.aau7735

Structure of the largest, most complex ribosome

Ribosomes are two-subunit ribonucleoprotein assemblies that catalyze the translation of messenger RNA into protein. Ribosomal RNAs (rRNAs) play key structural and functional roles. Ramrath *et al.* report the high-resolution structure of mitochondrial ribosomes from the unicellular parasite *Trypanosoma brucei* that contain the smallest known rRNAs. The trypanosomal mitoribosome is the most complex ribosomal assembly characterized, with two rRNAs and 126 proteins. The increased protein subunits have substituted for rRNA as an architectural scaffold. The structure also reveals the minimal core needed for ribosome function.

Science, this issue p. eaau7735